Small-Angle Scattering Study of Mesoscopic Structures in Charged Gel and Their Evolution on Dehydration

Masaaki Sugiyama*

Department of Physics, Kyushu University, Fukuoka 812-8581, Japan

Masahiko Annaka†

Department of Materials Technology, Chiba University, Chiba 263-8522, Japan

Kazuhiro Hara

Institute of Environmental Systems, Kyushu University, Fukuoka 812-8581, Japan

Martin E. Vigild

Danish Polymer Centre, Department of Chemical Engineering, Technical University of Denmark, 2800 Lyngby, Denmark

George D. Wignall

Condensed Matter Sciences Division, Oak Ridge National Laboratory, Oak Ridge, Tennessee 37831-6393

Received: December 20, 2002; In Final Form: April 18, 2003

Mesoscopic structures, with length scales $\sim 10^2$ Å, were investigated by small-angle X-ray and neutron scattering (SAXS and SANS) in several *N*-isopropylacrylamide−sodium acrylate (NIPA−SA) copolymeric hydrogels with varying [NIPA]/[SA] ratios and water contents. The SAXS experiments reveal that, depending upon the [NIPA]/[SA] ratio, the dehydrated NIPA−SA gel shows two mesoscopic structures: one consists of randomly distributed SA-rich islands in NIPA matrix, while the other is a microphase-separated structure, composed of NIPA-rich and SA-rich domains. In addition, the SANS experiments reveal the mesoscopic structural features during the dehydration process. As the concentration of the network polymers increases, NIPA-rich and water-rich domains segregate in the gel. Then, an electrostatic interaction between the segregated domains induces a microphase-separated structure in the limit of the dehydrated NIPA−SA gel.

I. Introduction

Nanostructures in multicomponent systems have been a longstanding interest for researchers in the fields of both fundamental science and technological applications. Some such systems undergo phase separation with decreasing compatibility among the constituents, and the consequent morphology is determined by a thermodynamic balance of the entropy of mixing and the surface energy.[1] For example, some homopolymer solutions phase separate on macroscopic ($>10^3$ Å) length scales, as a result of a coil−globule transition.[2] With the decrease in compatibility between polymer and solvent in the globule phase, the polymer minimizes its interfacial area with respect to the solvent and forms a coil, despite the fact that the induced macrophase separation decreases the entropy of mixing. When the system is composed of heteropolymers, as in the case of surfactants, a microphase separation occurs so as to increase the entropy of mixing. Surfactant systems exhibit a variety of morphologies in thermodynamic balance from lamellae to multicontinuous microemulsions.[3]

A gel is a system composed of a cross-linked polymer network and solvent and is therefore a multicomponent system. When the constituents are highly compatible with each other, the polymer network spreads out into the solvent to maximize the entropy of mixing. Conversely, the network shrinks to minimize the surface energy when the constituents are incompatible. For example, with increasing temperature, a homopolymer hydrogel of *N*-isopropylacrylamide (NIPA) exhibits a continuous volume reduction at 36 °C as the hydrophilic NIPA group turns hydrophobic. This phenomenon is well-known as the *volume phase transition*,[4,5] and the mesoscopic structural change in the NIPA gel in this transition (which results from enhancement of the static and dynamic fluctuations) has been observed via small-angle neutron scattering (SANS).[6]

When the polymer network is composed of monomers with different solvent compatibility, the behavior of the gel is more complicated. For example, in hydrogels composed of *N*-isopropylacrylamide and acrylic acid (NIPA−AAc) segments, the volume changes of the NIPA and AAc groups act in opposite directions as the temperature is increased. The NIPA groups turn from hydrophilic to hydrophobic, and at higher temperatures, this generates a contractive force within the polymer network, while the AAc groups induce an expansive force due to a positive osmotic pressure, which comes from the thermal motion of counterions in the Donnan potential.[5] Therefore, compared with the pure NIPA gel, the NIPA−AAc gel has an

* To whom correspondence should be addressed. Electronic address: sugi8scp@mbox.nc.kyushu-u.ac.jp.

† Present address: Department of Chemistry, Kyushu University, Fukuoka 812-8581, Japan.

10.1021/jp0277816 CCC: $25.00
Published on Web 06/10/2003

additional force that resists shrinking and exhibits a more steplike volume change at the higher transition temperature than does the pure NIPA gel.[7,8] In addition to these macroscopic features, it is also interesting to consider the structure of the NIPA−AAc gel from the mesoscopic point of view. Just below the transition point of the NIPA−AAc gel (at 50 °C), the AAc groups are hydrophilic, while the NIPA groups are hydrophobic. Therefore, the NIPA groups tend to associate with each other by expelling the solvent from the network, while the AAc groups attract the solvent. However, the constraint of electroneutralization inhibits the formation of macroscopic inhomogenieties in the solvent distribution of the hydrogel. As a result of the balance between the aggregation of like monomers and the constraint of electroneutralization, the NIPA−AAc hydrogel at this temperature would be expected to exhibit an inhomogeneous solvent distribution on mesoscopic length scales, and this is consistent with the observation of a microphase-separated structure composed of NIPA- and AAc-rich domains via SANS.[9,10]

This paper explores the property changes induced in a gel by dehydration and describes another mechanism (along with the *volume phase transition*) to produce a shrunken gel. In addition to overall decreases in volume, other properties show drastic changes during dehydration and the gel exhibits a glasslike behavior.[11] This has been confirmed with viscoelastic measurements,[12,13] via the observation of a low-frequency peak in Raman scattering,[14] and also by inelastic neutron scattering experiments.[15] Furthermore, a recent small-angle X-ray scattering (SAXS) study reveals a distinct mesoscopic structure in one heteropolymer hydrogel [*N*-isopropylacrylamide−sodium acrylate (NIPA−SA)], which exhibits microphase separation upon dehydration.[16] We believe that the solvent affinity of the NIPA group does not change appreciably because the dehydration was conducted at room temperature. Thus, we anticipate that microphase separation of heteropolymer gels is a general phenomenon, which is not restricted to the *volume phase transition*, and requires a balanced set of gel constituents with competing solvent affinities. Verifying the concrete conditions for microphase separation in a heteropolymer gel may lead to the ability to control the mesoscopic structure and to future technological applications.

There are many adjustable parameters to control the mesoscopic structure of the heteropolymer gel: choice of monomers for gelation, their ratio, concentration of solvent, counterions, cross-linkers, etc. In this paper, we will investigate the effect of the polymer ingredient ratio and also the water content on the mesoscopic structure of the NIPA−SA gel. As an initial step, SAXS profiles of dehydrated NIPA−SA gels at the several [NIPA]/[SA] ratios were measured. X-rays are sensitive to the distribution of SA, which has a greater scattering length density (11.2×10^{10} cm^{-2}) than NIPA (10.2×10^{10} cm^{-2}).[17] Then, to clarify how varying the proximity of network chains induces the mesoscopic structure, the evolution of SANS profiles of the NIPA−SA gel was observed at several water contents. Neutrons are very sensitive to the distribution of (heavy) water because of its large scattering length density (6.37×10^{10} cm^{-2})[17] in comparison with NIPA (1.43×10^{10} cm^{-2}) and SA (1.99×10^{10} cm^{-2}). Last, to investigate the influence of the solvent affinity of the NIPA group on the mesoscopic structure, SANS profiles of the pure NIPA and NIPA−SA gels were measured and compared with each other at temperatures in the hydrophilic (20 °C) and hydrophobic phases (40 °C).

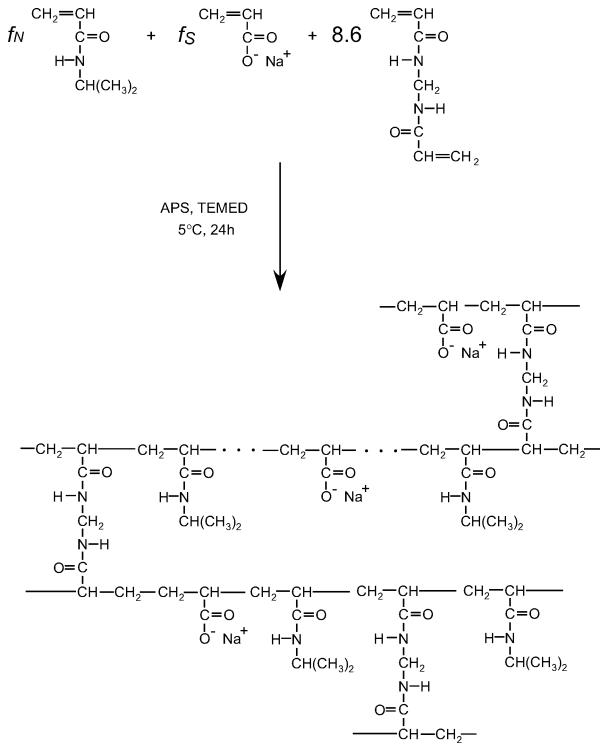

Figure 1. Preparation for the NIPA−SA gel and its chemical structure. In the gel network, NIPA, SA monomers, and BIS are randomly distributed. All specimens were prepared with $f_N + f_S = 700$ mM and 8.6 mM BIS concentration.

II. Experiments

A. Specimens. The solvents in the specimens for SAXS and SANS experiments were the light and heavy water, respectively. The aqueous solution of NIPA (f_N mM), SA (f_S mM), *N*,*N*′-methylene-bisacrylamide (BIS, 8.6 mM), and *N*,*N*,*N*′,*N*′-tetramethylethylenediamine (240 μL for 100 mL solution) was fully saturated with nitrogen; the specimens in the present study were prepared with $f_N + f_S = 700$. Then a small amount of ammonium persulfate (40 mg for 100 mL solution) was added into the mixture solution to initiate the gelation, which was carried out at 5 °C for 24 h. The preparation for the NIPA−SA gel and its chemical structure are illustrated schematically in Figure 1. We synthesized the NIPA−SA gels at several [NIPA]/[SA] ratios ($0 \le f_S \le 700$). After completion of the gelation reaction and the subsequent rinse-out of unreacted ingredients, several sections of wet NIPA−SA gel were cut and dried gently for 6 days in air. During this dehydration, the wet and soft gel turned into a hard and transparent glasslike material. We used these dehydrated gels as specimens in the SAXS experiments.

For the SANS experiments, specimens were prepared by adding controlled amounts of the heavy water to the dehydrated NIPA−SA gels to examine the dependence of the mesoscopic structure on the water content, which was indicated by R_{wp}, defined by the weight ratio of water (w) to the network polymer (p),

$$R_{wp} = \frac{M_S - M_D}{M_D} \tag{1}$$

where M_S is the weight of the specimen including solvent (water) and M_D is the weight of the specimen after complete desiccation at 100 °C for 1 h (which is considered to be the weight of the network polymer). For example, R_{wp} was around 0.3 in the NIPA−SA gel of $f_S = 200$ dried gently in air for 6 days,

TABLE 1: Samples for SAXS and SANS Experiments

SAXS[a]		SANS		
code	f_s	code	f_s	R_{wp}
A	0	K	200	fully wet[b]
B	100	L	200	8.1
C	200	M	200	5.5
D	250	N	200	2.9
E	300	O	200	1.6
F	350	P	200	1.3
G	400	Q	200	1.0
H	500	R	200	0.3[a]
I	600	S	0	fully wet[b]
J	700	T	0	1.3

[a] Dehydrated gel. [b] As prepared.

which indicates that there remains some bound water.[14] All of the specimens investigated in the present study are listed in Table 1.

B. Small-Angle X-ray Scattering. We conducted the SAXS experiments of the dehydrated NIPA−SA gels at several [NIPA]/[SA] ratios (samples A−J) to elucidate how the polymer ingredient ratio influences the mesoscopic structure. The experiments were carried out at room temperature with a SAXS apparatus (SAXES) installed at BL10C of Photon Factory in Institute of Materials Structure Science (IMSS), High Energy Accelerator Research Organization (KEK), Tsukuba, Japan. An X-ray beam (1.488 Å in wavelength) was used as a light source of SAXES, and the intensity distribution of the scattered X-ray was measured by a one-dimensional position-sensitive detector. The magnitude of the scattering vector ($q = (4\pi/\lambda)\sin(\theta/2)$, where λ is the wavelength and θ is the angle of scatter) ranged from 6.0×10^{-3} to 1.5×10^{-1} Å^{-1}. The observed X-ray intensity was corrected for the cell scattering and absorption and then normalized with respect to the thickness of the sample and irradiation time. The net data are proportional to the differential scattering cross sections and may therefore be used for quantitative comparisons between samples with different thicknesses.

C. Small Angle Neutron Scattering. SANS experiments were conducted to investigate the evolution of the mesoscopic structure as the water content decreases. The specimens were NIPA−SA gels of $f_S = 200$ at several water contents (fully wet gel and $8.1 \geq R_{wp} \geq 0.3$, samples K−R). The fully wet pure NIPA gel (sample S) was also measured for reference. The SANS experiments were performed at room temperature with the 30 m SANS instrument installed at the High Flux Isotope Reactor at Oak Ridge National Laboratory (ORNL), Tennessee.[18] The incident neutron beam was monochromatized to be 4.75 Å, and the scattered neutrons were observed with a two-dimensional position-sensitive detector. The magnitude of the scattering vector ranged from 1.0×10^{-2} to 1.0×10^{-1} Å^{-1}. The observed scattering intensity was corrected for the cell scattering and absorption, normalized with respect to sample thickness and measuring time, and converted to an absolute differential cross section (in units of cm^{-1}) by comparison with precalibrated standards.[19] The measured cross section subdivides into coherent and incoherent components, and only the former contains information on the structure of the sample. The incoherent cross section forms an isotropic background, which must be subtracted, and because D_2O produces virtually no incoherent signal, this correction was estimated from the (flat) asymptotic limit of the high-q region (∼0.08 Å^{-1}) of the dry samples. This correction was small compared to both the observed $I(0)$ values (∼5 cm^{-1}) or peak heights (∼30 cm^{-1}), and typical backgrounds subtracted were ∼0.4 cm^{-1} to give the net coherent cross section of the samples.

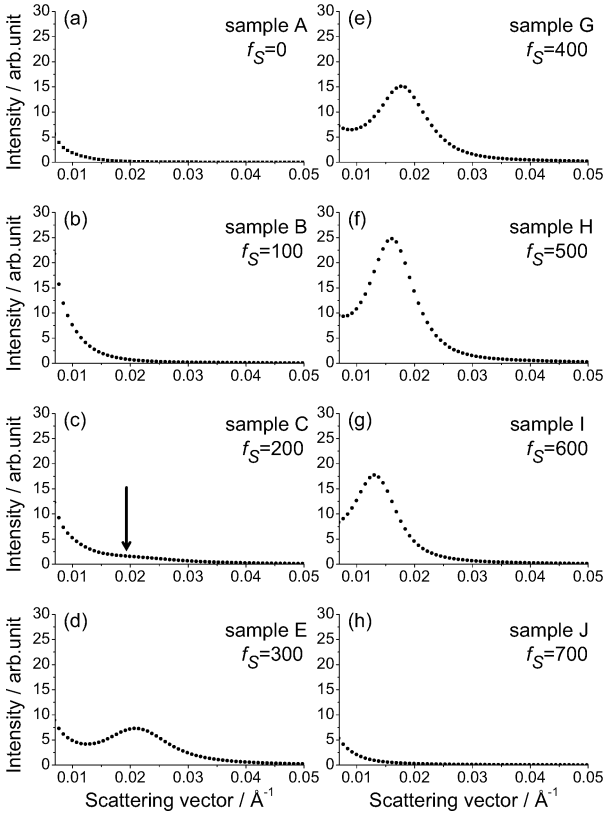

Figure 2. SAXS profiles of the dehydrated NIPA−SA gels at several [NIPA]/[SA] ratios: (a) sample A (a pure NIPA gel, $f_S = 0$); (b) sample B ($f_S = 100$); (c) sample C ($f_S = 200$); (d) sample E ($f_S = 300$); (e) sample G ($f_S = 400$); (f) sample H ($f_S = 500$); (g) sample I ($f_S = 600$); (h) sample J (a pure SA gel, $f_S = 700$). An arrow in panel c indicates the position of a faint peak. See also text.

To investigate the hydrophobicity effect of NIPA groups on the microphase separation, we performed temperature-controlled experiments. The chosen samples (samples P and T) were all of a low water content ($R_{wp} = 1.3$). Measurements were performed with a SANS instrument (KUR−SANS) installed at Kyoto University Reactor in Research Reactor Institute of Kyoto University (KURRI), Osaka, Japan.[20] The incident neutron beam was monochromatized to be 5.6 Å, and the scattered neutrons were observed with a two-dimensional position-sensitive detector. The magnitude of the scattering vector ranged from 1.1×10^{-2} to 1.6×10^{-1} Å^{-1}. The temperature drift of the specimen was controlled to be within 0.2 °C around target temperatures by utilizing a temperature-controlled water circulation equipment (Lauda 206E). In a series of the temperature-variation SANS experiments, the profile measurements were performed after waiting for thermal equilibrium (by waiting at the target temperature for 5 h). The data corrections were performed in the same manner as described above, with the exception of conversion to an absolute scale.

III. Results and Discussion

A. Mesoscopic Structures of Differently Composed Dehydrated NIPA−SA Gels. We first consider the relation between the observed mesoscopic structure and the [NIPA]/[SA] ratio as revealed in the SAXS experimental results of the dehydrated gels (samples A−J). As shown in Figure 2a, the profile of sample A is almost flat except for a weak diffuse scattering observed in the lower q-region ($q < 0.02$ Å^{-1}). In particular, there is no peak in either the SAXS profile of this pure dehydrated NIPA gel or the dehydrated NIPA−SA gel with

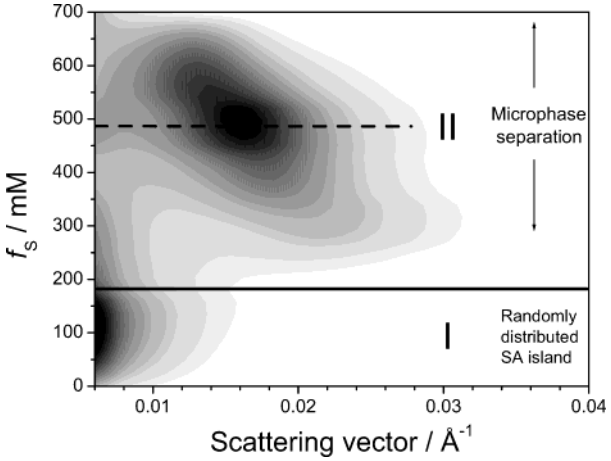

Figure 3. [NIPA]/[SA] dependence of the SAXS profiles of the dehydrated NIPA−SA gel. Density corresponds to the SAXS intensity. See also text.

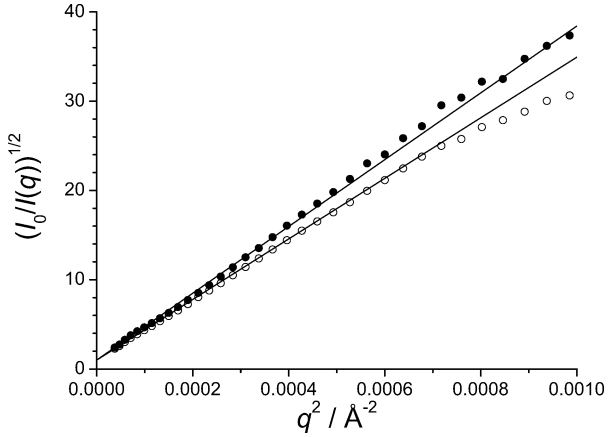

Figure 4. Debye−Bueche analyses of SAXS profiles at $f_S = 0$ and 100: (●) sample A ($f_S = 0$); (○) sample B ($f_S = 100$). The straight lines are the results of least-squares fittings with eq 2; their slopes correspond to the square of the correlation length. See also text.

small SA concentration (sample B; $f_S = 100$), though the diffuse tail in the lower q-region of the latter becomes more intense (Figure 2b). With increasing SA concentration (sample C; $f_S = 200$), the diffuse tail in the lower q-region weakens and a faint peak (indicated by the arrow in Figure 2c) emerges around 0.02 Å^{-1}. With further increases in SA concentration (samples D−I), an apparent peak appears and varies in intensity as indicated in Figure 2d−g. For increasing values of SA concentration, the peak position shifts toward lower q monotonically, while the peak intensity increases and shows a maximum at $f_S = 500$ (sample H), after which it decreases. As shown in Figure 2h, the SAXS profile of the pure SA gel (sample J) exhibits no peak except for the diffuse tail in the lower q-region, similar to that of the pure NIPA gel.

These characteristics of the [NIPA]/[SA] ratio influence on the SAXS profiles are illustrated in Figure 3, which shows that there is a notable change in the SAXS profile around $f_S = 200$. Therefore, the mesoscopic structure of the dehydrated NIPA−SA gel can be classified into following two regions: regime I is in a range of f_S from 0 to 200, and regime II is in a range from 200 to 700.

The pure dehydrated NIPA gel should be almost homogeneous in a mesoscopic scale because its SAXS profile has no peak except for a weak diffuse tail in the low q-region. The scattering function of an uncharged wet gel is well-described with a combination of scattering factors originating from solidlike (static) and liquidlike (dynamic) density fluctuations.[21,22] The static fluctuations come from an inhomogeneous distribution of cross-links of the polymer network introduced in the gelation process. The dynamic fluctuations come from thermal fluctuations of the polymers between the cross-links.[22] In the dehydrated gels, the liquidlike scattering factor should be negligible[23] because the motion of the chain segments is restricted by the glasslike state of the system. Hence the observed diffuse tail should result from static density fluctuations, and following the Debye−Bueche formalism for two-phase systems,[24,25] we can describe the scattering intensity as

$$I(q) = \frac{I_0}{(1 + \xi_s^2 q^2)^2} \qquad (2)$$

where ξ_s is a correlation length of the static density fluctuation. As shown in Figure 4, the SAXS profile of the pure dehydrated NIPA gel (closed circles) is well-described by eq 2. The straight line is the result of a least-squares fit of the data to eq 2, and the slope is proportional to the square of the correlation length, which is estimated to be 193 ± 3 Å. This result is consistent with the existence of a density distribution with a correlation length of ∼190 Å in the polymer network of the dehydrated NIPA gel.

The polymer−polymer interaction should become dominant with evaporation of the solvent, and as the distance between the network polymer segments decreases, the SA groups would be expected to aggregate during the dehydration process in NIPA−SA gels with small SA concentration. Figure 2b shows that the intensity of the diffuse scattering of sample B ($f_S = 100$) becomes more intense compared to sample A, probably owing to the increase in the scattering contrast between the NIPA-rich matrix (high-density domain of the NIPA) and the SA-rich domain. Also in comparison to sample A, the correlation length of sample B (estimated from open circles in Figure 4 to be 184 ± 2 Å) is close to that of the pure dehydrated NIPA gel. These experimental results suggest that the structure in the two-component dehydrated NIPA−SA system may reflect the inhomogeneities in the one-component gel. Thus, for small SA concentration, the SA-rich domains in the dehydrated NIPA−SA gel may have a similar spatial distribution to the low-density regions of the pure NIPA gel. This inhomogeneous structure, with randomly distributed mesoscopic SA-rich islands in the NIPA-rich matrix, can be regarded as a characteristic structural feature of regime I in Figure 3.

With the increase of SA concentration, the size of the SA-rich islands becomes larger, though they cannot grow to macroscopic length scales (>10^3 Å) because of restrictions of the electroneutrality and the pinning or entanglement of the polymer network or both. Therefore, the build-up of SA islands should cease when the size of the islands reaches mesoscopic (∼10^2 Å) length scales. The emergence of the peak in regime II should reflect the occurrence of microphase separation. The position and intensity vary with SA concentration as shown in Figure 5. With increasing SA concentration, the size of the SA-rich domains should become larger, which is signaled by the peak shift toward the lower q-region. The scattering intensity is proportional to the contrast between SA-rich and NIPA-rich domains and reaches a maximum when the volume factions of two phases become equal.[24,25] In the dehydrated NIPA−SA gel, the NIPA- and SA-volume fractions in the polymer network may be estimated (via their densities) to be equal at $f_S = 410$, which is very close to the ratio at which the peak intensity exhibited maximum in Figure 3 ($f_S = 480$).

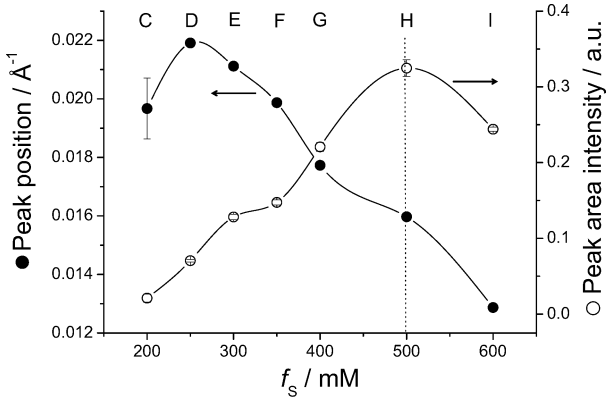

Figure 5. Evolution of the SAXS peak position and intensity with SA concentration in regime II: (●) peak position; (○) intensity. Symbols indicate the sample codes. See also text.

In this section, we have postulated the occurrence of inhomogeneities to explain the diffuse scattering in the low q-region and the emergence of a peak in the SAXS profile of the dehydrated NIPA−SA gel. These indicate a distinct mesoscopic structure, and in the following sections, we will examine the possible mechanisms that give rise to such inhomogeneities during the dehydration process.

B. Mesoscopic Structural Evolution with Water Content. *1. SANS Profile Analysis.* To accomplish this purpose, to examine the role played by the distribution of water within the mesoscopic structures, it is important to study NIPA−SA gels with low water contents. For this purpose, we performed the SANS experiments of the NIPA−SA gels ($f_S = 200$) at several water contents: the fully wet gel and $8.1 \geq R_{wp} \geq 0.3$ (samples K−R).

As shown in Figure 6a, the SANS profile of the wet NIPA−SA gel (sample K) is almost flat, apart from a low-intensity contribution from thermal density fluctuations. This indicates a homogeneous structure, and to obtain the correlation length describing the thermal fluctuations, we employed the Ornstein−Zernike formalism,

$$I(q) \approx \frac{1}{(1 + \xi_d^2 q^2)} \tag{3}$$

where ξ_d is the correlation length of the thermal density fluctuations, which may be estimated by fitting eq 3, ξ_d, to be 18 Å. In comparison, fitting eq 3 to the SANS profile (not shown) of the fully wet NIPA gel (sample S) gives $\xi_d = 30$ Å. This indicates that electrostatic interactions between the acrylate group and counterion may suppress the thermal motion of the network polymer.[26,27]

As shown in Figure 6b,c, the intensity in the low q-range increased with decreasing the water content, which suggests the presence of a fluctuation in scattering length density related to the water distribution in the gel. Because the SANS profiles were found not to be consistent with the Ornstein−Zernike-type correlation function (eq 3), these fluctuations could not result from the simple thermal density fluctuation of the network polymers. As the water content is further decreased (samples N and O), a peak emerges around $q = 0.02$ Å^{-1} as shown in Figure 6d,e. The peak intensity increases with the reduction in R_{wp} and reaches a maximum around $R_{wp} = 1.3$ (sample P, Figure 6f); then the peak weakens again (sample Q, Figure 6g). Finally, the peak becomes very weak (sample R, Figure 6h), and a diffuse tail is observed in the low q-region, similar to the SAXS profile of the dehydrated gel (sample C, Figure 2c).

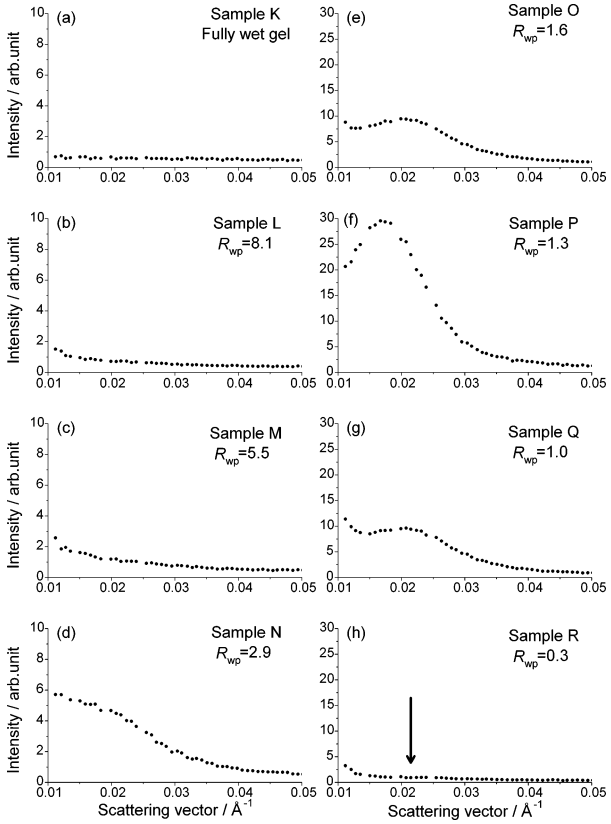

Figure 6. SANS profiles of the NIPA−SA gels of $f_S = 200$ at several water contents: (a) sample K (a fully wet gel); (b) sample L ($R_{wp} = 8.1$); (c) sample M ($R_{wp} = 5.5$); (d) sample N ($R_{wp} = 2.9$); (e) sample O ($R_{wp} = 1.6$); (f) sample P ($R_{wp} = 1.3$); (g) sample Q ($R_{wp} = 1.0$); (h) sample R (dehydrated gel, $R_{wp} = 0.3$). The magnification of vertical scale in panels e−h is reduced to one-third of that in panels a−d. An arrow in panel h indicates the position of a faint peak.

From the evolution of the SANS profiles as described above, the mesoscopic structural evolution with decreasing water content can be classified into three stages. The first stage is in the range of $R_{wp} \geq 5.5$ (samples L and M) and is characterized by a diffuse tail in a low q region. The second stage in the range of $5.5 > R_{wp} \geq 1.3$ (samples N−P) is characterized by the emergence of a peak, and the third stage in the range of $R_{wp} < 1.3$ (samples Q and R) is where the peak diminishes. The evolution of the SANS peak position and intensity with water content in the second and third stages are shown in Figure 7.

We will now discuss the structural changes associated with stages 1−3, which are illustrated schematically in Figure 8. In the wet NIPA−SA gel, it might be expected that a strong electric force due to full dissociation of the SA group should suppress the mesoscopic inhomogeneity as shown in Figure 8a, and there is no peak in the SANS profile (Figure 6a). In addition, the osmotic pressure from the motion of counterions and water molecules expands the whole volume of the gel in air. With decreasing water content (and osmotic pressure), the network polymers approach each other and similar groups tend to aggregate. With this development, the NIPA-rich domains should become rather hydrophobic because the interaction χ-parameter of NIPA and water decreases with increasing polymer concentration.[8] Thus, the emergence of randomly distributed NIPA-rich islands of low water content would induce a fluctuation in the water distribution and give rise to a mesoscopic structure composed of randomly distributed NIPA-rich domains in the water-rich environment (Figure 8b), which might account for the SANS profiles in the first stage (samples

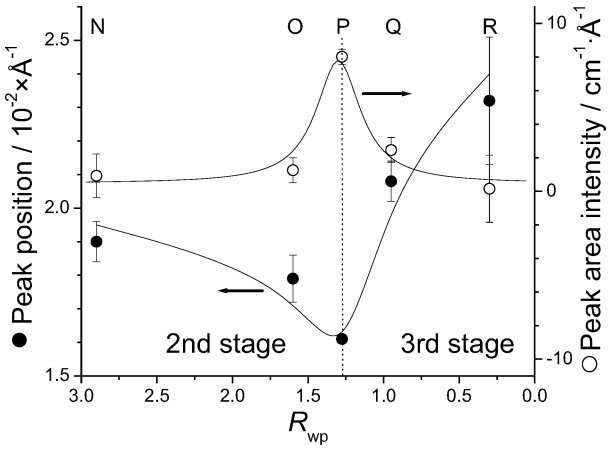

Figure 7. Evolution of the SANS peak position and intensity with water content in the second and third stages (samples N−R): (●) peak position; (○) intensity. Symbols indicate the sample codes.

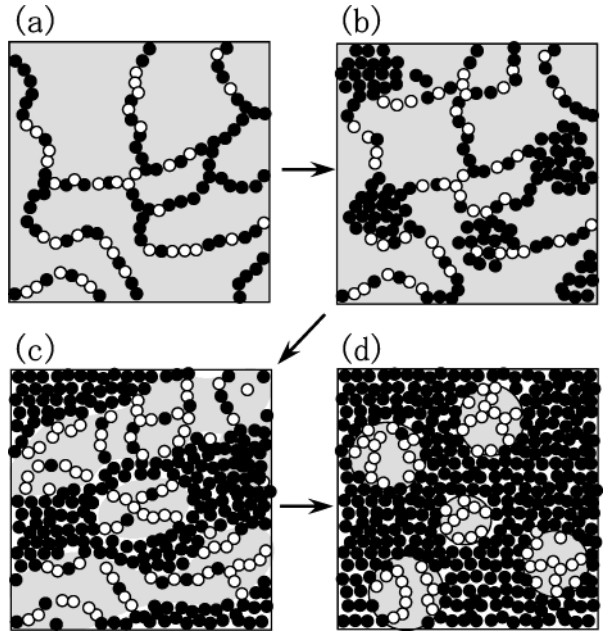

Figure 8. Illustration of structural evolution on dehydration: (●) NIPA monomers; (○) SA monomers; (gray regions) water-rich domains: (a) a wet gel (stage 1); (b) the gel in stage 2, where the NIPA-rich islands are developing; (c) the gel at a phase inversion between the NIPA-rich and the water-rich (sample P, $R_{wp} = 1.3$); (d) the gel in stage 3, where water-rich islands distribute in a NIPA-rich matrix.

L and M). As the water content is decreased, the water-rich domains gradually shrink in response to forces arising from the osmotic pressure, allowing the hydrophobic NIPA-rich islands to grow. It should be noted that to preserve the electrostatic neutrality and a homogeneous osmotic pressure, the uncharged NIPA-rich domains must be distributed uniformly and this implies that the distances between the neighborhood NIPA islands should be approximately the same. This would be reflected in a peak in the SANS profile in the second stage (samples N−P, $5.5 > R_{wp} > 1.3$), as shown in Figure 6d−f. Following this line of argument, we may estimate the interdomain distance ($\sim 2\pi/q_{peak}$) of the gels in the second stage to be ~300 Å (Figure 7). Thus, the second stage will be characterized by such a microphase-separated structure, and as the separation proceeds further with decreasing water content, the NIPA-rich domain size will approach that of the water-rich domain (Figure 8c) and the peak intensity will be maximized as shown in Figure 7 (sample P, $R_{wp} = 1.3$).

As the water content is further decreased, a phase inversion should occur between the NIPA-rich and the water-rich phases and results in a dispersion of water-rich islands in a NIPA-rich matrix (Figure 8d). Supporting this structural interpretation in the third stage, the SANS peak position shifts toward the higher q-range and the intensity weakens with decreasing the water content as shown in Figure 7 (samples Q and R, $R_{wp} < 1.3$).

2. Phase Diagram. As described in the previous section, the osmotic pressure due to an electrostatic interaction between acrylic acid groups and counterions appears to play an important role in the mesoscopic structural change that occurs during dehydration, and this calls for a further examination of the effect of the electrostatic interaction during the dehydration process.

Theoretical discussions of the behavior of polyelectrolyte polymers in poor solvents have been given by Borue and Erukhimovich[28] and by Joanny and Leibler,[29] and these theories have been successfully applied to explain the SANS profiles from weakly charged gels in a poor solvent.[9,30,31] We will therefore employ the Borue and Erukhimovich (BE) theory to analyze the observed SANS profiles and to examine the electrostatic interaction in the NIPA−SA gel during the dehydration process. According to the BE theory, the scattering intensity can be formulated in terms of reduced quantities of the scattering vector, **x**, salt concentration, s, and temperature (or solvent quality), t, as follows:

$$I(q) \approx \frac{1}{(\mathbf{x}^2 + t) + 1/(\mathbf{x}^2 + s)} \tag{4}$$

The reduced scattering vector **x** is derived by the characteristic screening length of electrostatic interaction in salt-free solution, r_0, as

$$\mathbf{x} = r_0 q \tag{5}$$

The characteristic length, r_0, is the scale length of the system and relates to the charge density ρ as follows:

$$r_0 = a(48\pi\alpha a^2 L\rho)^{-1/4} \propto \rho^{-1/4} \tag{6}$$

where α, a, and L are the degree of ionization, segment length of monomer, and Bjerrum length ($L = e^2/(4\pi\epsilon k_B T)$, e = elementary electric charge, ϵ = dielectric constant of solvent, k_B = Boltzmann's constant, T = temperature), respectively. The reduced salt concentration, s, is a function of the scale length, r_0, and Debye screening length, r_s, and is given by

$$s = \frac{r_0^2}{r_s^2} \tag{7}$$

The value of s indicates the degree of the electrostatic screening, and with increasing salt concentration, the Debye screening length, r_s, becomes shorter, so s increases. The reduced temperature, t, in a poor solvent is a function of r_0, a, and the Flory interaction parameter, χ, and is defined by

$$t \cong 12\left(\frac{r_0}{a}\right)^2 (1 - 2\chi) \tag{8}$$

The SANS profiles of samples L−Q are well described by eq 4 with the exception of the fully wet and dehydrated gels (samples K and R). Typical fits to SANS data sets with and without a peak are shown in Figure 9a,b, where x, s, and t were used as fitting parameters.

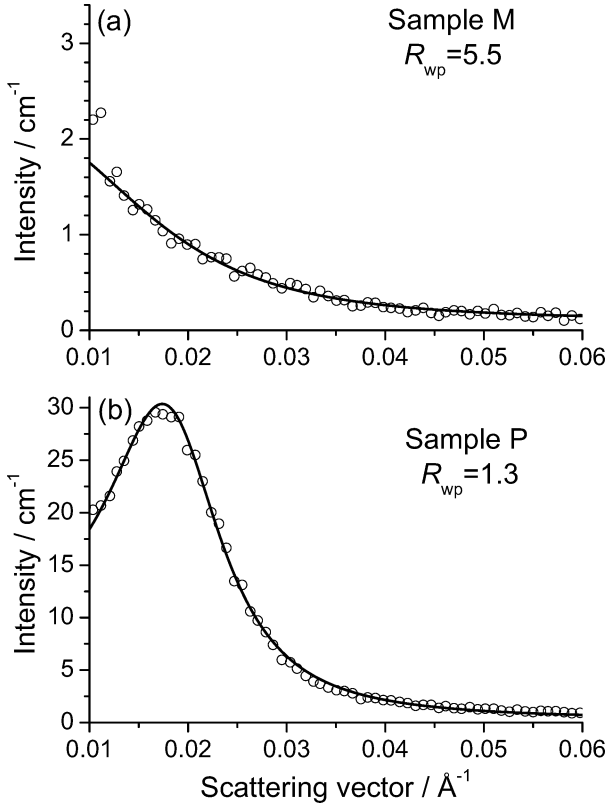

Figure 9. Typical examples of the fitting results of the SANS profiles with BE theory: (a) sample M (without a peak, $R_{wp} = 5.5$); (b) sample P (with a peak, $R_{wp} = 1.3$). Thick lines indicate the results of the least-squares fittings after BE theory (eq 4).

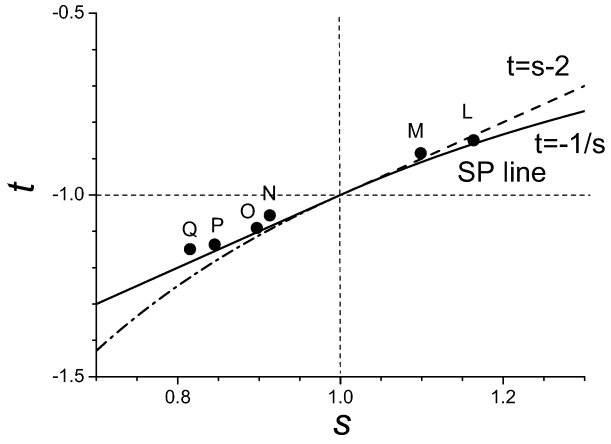

Figure 10. Locations of the NIPA−SA gels at several water contents in the $s-t$ phase diagram after BE theory. Parameters s and t are reduced quantities of salt concentration and temperature, respectively. Thick line denotes a spinodal line. Closed circles indicate the samples in the present SANS experiment, and the characters above the circles denote their sample codes.

From the BE perspective, the character of the partially dehydrated NIPA−SA gels may be illustrated with respect to an $s-t$ phase diagram, which is divided into 10 regimes by $|t - s| = 2$, $|st| = 1$, and other lines.[28] Figure 10 shows the location, in a part of the $s-t$ phase diagram, of the partially dehydrated NIPA−SA gels of different water contents (samples L−Q), which correspond to the poor solvent regime ($t < 0$) in BE theory.[28] In Figure 10, the thick line indicates the spinodal line, which is defined by $t = s - 2$ in a range of $s < 1$ and $t = -1/s$ for $s > 1$. Below the spinodal line, the system shows phase separation and this region may be further divided into microphase ($s < 1$) and macrophase ($s > 1$) separated subsections. At the critical point, where the lines of $s = 1$ and $t = -1$ meet, the electrostatic interaction is completely unscreened.

With decreasing the water content, location of the NIPA−SA gels shifts along the spinodal line in the $s-t$ phase diagram toward the critical point. As the polymer concentration increases, the solvent becomes poorer,[8] and t decreases according to eq 8. It should be noted that the density of electric charge increases during dehydration, which results in a reduction in r_0 via eq 6. Therefore, both t and s decrease during the dehydration. When the distance between the network polymers is longer than the effective range of the electrostatic interaction, r_s, the system corresponds to the region of the phase diagram where $s \gg 1$. As the polymer density increases, thus reducing t and s, the polymer network segments approach one another. When the effective range of the electrostatic interaction and the distance between segments overlaps, this should give rise to a density fluctuation (samples L and M). Between samples M and N, the locus of the dehydrating gel in the phase diagram passes through the critical point. In the regime of $s < 1$, the effective range of the electrostatic interaction strongly overlaps and the system exhibits a microphase separation, evidenced by a scattering intensity maximum at a finite q in the SANS profile (samples N−Q). Further reduction of the water content in the NIPA−SA gel means that both of t and s decrease and that the location of the NIPA−SA gel in the phase diagram shifts along the spinodal line.

The preceding discussion suggests that an unscreened electrostatic interaction can play a very important role to induce a microphase separation in the dehydrated NIPA−SA gel, according to the BE theory. It follows from the preceding considerations that the gel with the high salt concentration should not exhibit the microphase separation because the electrostatic interaction should be completely screened and r_s should be very short. In a preliminary experiment, the dehydrated NIPA−SA gel of $f_S = 300$ was found not to exhibit a microphase separation when a NaCl solution was introduced into the gel prior to dehydration. The characteristics of the NIPA−SA gel on the dehydration can be summarized as follows: The dehydration induces the polymer condensation, increase in χ of NIPA groups for water molecules, and consequently decrease in t and s, owing to eqs 5−8. When s becomes smaller than 1, the gel exhibits a microphase separation. Alternatively, the condensation of the polymer network induces inhomogeneities, and as a result, overlapping the effective range of the electrostatic interaction induces a microphase separation of the NIPA−SA gel.

C. Effect of Hydrophobicity of NIPA on Structure. To examine the effects on the mesoscopic structure of the hydrophobicity of NIPA groups and of electrostatic interaction between SA groups, further experiments were conducted on two specimens. A pure NIPA gel (sample T) and a NIPA−SA gel of $f_S = 200$ (sample P), both with a small amount of water ($R_{wp} = 1.3$), were studied as a function of temperature via SANS. After water was added, both gels were slightly swollen but remained transparent at 20 °C. It should be noted that, at this temperature, the electrostatic interaction among the SA groups in sample P is unscreened and most of the NIPA groups are hydrophilic. To increase the hydrophobicity of the NIPA groups, the temperature was raised and held at 40 °C for 5 h. At this temperature, the pure NIPA gel (sample T) became opaque, while the NIPA−SA gel (sample P) remained transparent. These observations indicate that after adding a small amount of water, the pure NIPA gel becomes heterogeneous

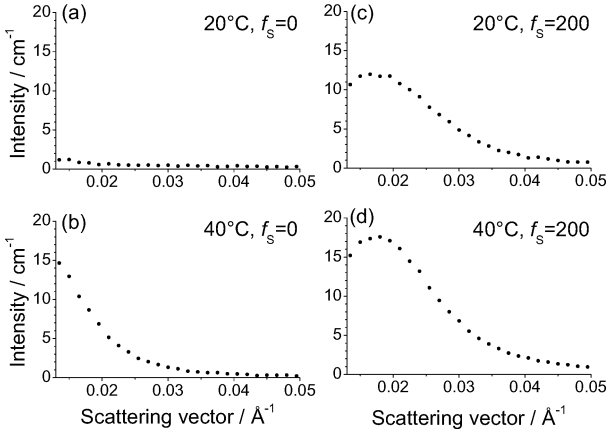

Figure 11. Temperature dependence of the SANS profiles: (a) the pure NIPA gel (sample T, $f_S = 0$) at 20 °C; (b) the pure NIPA gel (sample T, $f_S = 0$) at 40 °C; (c) the NIPA−SA gel (sample P, $f_S = 200$) at 20 °C; (d) the NIPA−SA gel (sample P, $f_S = 200$) at 40 °C.

while the NIPA−SA gel remains homogeneous on length scales of the order of the wavelength of light at 40 °C.

Figure 11 shows SANS profiles of the pure NIPA and the NIPA−SA gels (samples T and P) at 20 and 40 °C. At 20 °C, the NIPA−SA gel shows a peak (Figure 11c) indicating microphase separation, while the SANS profile of the pure NIPA gel at same temperature is almost flat, reflecting a homogeneous structure (Figure 11a). At 40 °C, the intensity around the low q region increases substantially in the pure NIPA gel (Figure 11b), which could reflect the segregation between the network polymer and water due to increase in the hydrophobicity of the NIPA groups. It should be recalled that the pure NIPA gel exhibits no electrostatic interaction that generates a resistive force against condensation of the polymer network. Therefore, the pure NIPA gel does not exhibit microphase separation, though the density fluctuation correlation length can increase to length scales comparable to the wavelength of light. Such behavior is demonstrated in Figure 11b via an intense tail in the low q region without a distinctive peak at a finite q. This viewpoint is supported by the BE theory described in the previous section (section III.B.2). In the $s-t$ phase diagram, the pure NIPA gel is located in the range of $s \gg 1$, where the electrostatic interaction is completely screened. Therefore, the temperature increase induces a decrease of t, and *macrophase* separation occurs as the locus shifts below the spinodal in Figure 10.

For the NIPA−SA gel, the peak position remains virtually unchanged as the temperature is increased, though the intensity increases at 40 °C as shown in Figure 11d. This could indicate an enhancement of the scattering contrast between NIPA-rich and water-rich domains without a large structural change. The reduction of the water affinity to the NIPA groups should tend to drive the water out of the NIPA-rich domain generating a volume decrease of the gel. At the same time, the osmotic pressure due to motion of counterions should increase with temperature and stabilize the mesoscopic structure. As a result, the contrast between the NIPA-rich and water-rich (i.e., SA-rich) domains should become higher, thus increasing the peak intensity as shown in Figure 11d. According to this interpretation of the SANS results, the heterogeneity of the polymer network is the most important factor for inducing the microphase separation in the shrunken gel.

IV. Conclusions and Remarks

The results of the SAXS experiments on the mesoscopic structure dependence on the [NIPA]/[SA] ratio in dehydrated NIPA−SA gels can be summarized as follows: The dehydrated NIPA−SA gel exhibits two kinds of mesoscopic structure, which emerge in different SA concentration regimes. One regime is characterized by randomly distributed SA-rich islands in a NIPA-rich matrix. The other is a microphase-separated structure composed of NIPA-rich and SA-rich domains. The dehydrated pure NIPA gel shows a SAXS profile characteristic of static density fluctuations. In the dehydrated NIPA−SA gels with a small SA concentration component, the SA groups aggregate into water-rich domains with low-NIPA concentrations, which give rise to SA-rich islands during the dehydration process. As the SA concentration increases, the size of the SA-rich islands should become larger but would not be expected to reach macroscopic dimensions because of the constraints of electrical neutrality and the pinning or entanglement of the network polymer or both. This forces the dehydrated NIPA−SA gel to exhibit a microphase separation, which proceeds in three stages. During the first stage, randomly distributed hydrophobic NIPA-rich islands emerge in the water-rich environment. During the second stage with decreasing water, the NIPA-rich domains develop to a given size in the water-rich matrix and are evenly distributed to maintain electrical neutrality, thus creating a microphase-separated morphology as reflected by a peak in the SANS profiles. In the third stage, the phase inversion between the NIPA-rich and water-rich domains is thought to occur. Analyses based on BE theory indicate that the reduced salt concentration (or the degree of the screening of the electrostatic interaction), s, plays an important role in the microphase separation process. During the dehydration process, s becomes small because of proximity of the charged groups, as does the reduced temperature, t, because of increase in the hydrophobicity of NIPA-groups in the high-concentration NIPA domains. In the $s-t$ phase diagram, the locus of the NIPA−SA gel shifts along a spinodal line during dehydration, and when s becomes smaller than 1, the gel would show microphase separation. In other words, $s = 1$ is a boundary between the first and the second stages. From these results, a gel consisting of both charged and uncharged groups is predicted to show microphase separation on dehydration.

Temperature-changes should vary the hydrophobicity of the NIPA group and thus also influence the mesoscopic structure. As shown in Figure 11, increasing temperature reduces the water affinity to the NIPA group and induces inhomogeneity in the pure NIPA gel. However, unlike the NIPA−SA gel with low water content, the inhomogeneity develops to macroscopic length scales, possibly because of the lack of a restraining electrostatic interaction. In the NIPA−SA gel on the boundary between regimes I and II, where the shrinking force due to the hydrophobicity of the NIPA group competes with the expanding force from the electrostatic interaction, its mesoscopic structure does not change appreciably as the temperature is increased. Further experiments to elucidate the temperature dependence of the mesoscopic structure during the dehydration process are currently in progress.

It is interesting to note that, as shown in Figure 3, the dehydrated NIPA−SA gels with $f_S \leq 100$ do not show a microphase separation, while most wet NIPA−SA gels in this range exhibit a volume phase transition.[7,8] Conversely, NIPA−SA gels with $f_S > 100$ exhibit a microphase separation on dehydration but do not show volume phase transitions. This suggests that microphase separation and volume phase transitions may be mutually exclusive phenomena occurring in the NIPA−SA gel. While no definitive confirmation of this speculation has yet been achieved, we offer the following line

of argument: The gel volume in materials exposed to the atmosphere is maintained by the osmotic pressure due to the motion of the counterions and water molecules. As shown in Figures 2c and 6e,f, the NIPA−SA gel with $f_S = 200$, which does not show a volume phase transition, exhibits microphase separation in the conditions of both low water content and complete dehydration in air. Therefore, we propose that the microphase-separated structure could be an important factor in generating the homogeneous osmotic pressure that holds the gel volume at low water content.

As discussed in the Introduction, the NIPA−AAc gel of $f_S = 38$ shows a discrete volume decrease on the volume phase transition with increasing temperature.[9] Just below a critical temperature, the electrostatic interaction induces the microphase separation and, simultaneously, holds the volume.[9] On the other hand, above the critical temperature, the shrinking force overcomes the electrostatic force and thus induces a discrete volume decrease in the gel. There is no observation of the mesoscopic structure of NIPA−AAc gel in the shrunken phase, and the NIPA−SA gel of $f_S = 100$, which has an ingredient ratio of similar magnitude to the above-mentioned NIPA−AAc gel, does not show the microphase-separated structure in the present study (Figure 2b). Therefore, the mesoscopic structure with microphase separation should be destroyed in the shrunken gel with $f_S \leq 100$.

Finally, let us consider the many other parameters that should influence the mesoscopic structure of the dehydrated gel. Among them, the [NIPA]/[SA] ratio should have a considerable influence on the balance between the hydrophobic and the electrostatic interactions, and this parameter is most important for the development of microphase separation. Also, screening of the electrostatic interaction with addition of salt should deeply affect the origin and development of the microphase separation because, according to BE theory, excess counterions enhance the electrostatic screening and make *s* small. The concentration of cross-links should be another important parameter because it can influence the elasticity of the polymer network and the size of the microphase-separated domains. In fact, in a preliminary experiment, we found that the dehydrated NIPA−SA gel with the higher cross-link concentration than the present study exhibited a microphase separation with a smaller correlation length. For the purpose of controlling the mesoscopic structure in heteropolymer gels at will, further investigations of the effects of these parameters are of great importance and interest.

Acknowledgment. The authors express their thanks to Dr. H. Inoko of Osaka University for his kind help on the SAXS experiments. The SAXS experiments were performed under the approval of the Photon Factory Advisory Committee (Proposal No. 2000G242). The SANS experiments in ORNL were performed under the US-Japan Cooperative Research Program on Neutron Scattering, and we acknowledge this program. The work at Oak Ridge National Laboratory was also supported by the Division of Materials Sciences under Contract No. DE-AC05-00OR22725 with the Oak Ridge National Laboratory, managed by UTBattelle, LLC. The SANS experiments in KURRI were performed under Contract No. 14062. Financial support for M.E.V. is acknowledged from the J. C. Hempel's Foundation and the DANSCATT Center (Danish National Science Research Council).

References and Notes

(1) De Gennes, P. G. *Scaling Concepts in Polymer Physics*; Cornell University Press: Ithaca and London, 1979.
(2) Sun, S. T.; Nishio, I.; Swislow, G.; Tanaka, T. *J. Chem. Phys.* **1980**, *73*, 5971.
(3) Lindman, G. In *Surfactants*; Tadros, Th. F., Ed.; Academic Press: London, 1984.
(4) Tanaka, T. *Phys. Rev. Lett.* **1978**, *40*, 820.
(5) Tanaka, T. *Phys. Rev. Lett.* **1980**, *45*, 1636.
(6) Shibayama, M.; Tanaka, T. *J. Chem. Phys.* **1992**, *97*, 6829.
(7) Hirotsu, S.; Hirokawa, Y.; Tanaka, T. *J. Chem. Phys.* **1987**, *87*, 1392.
(8) Hirotsu, S. *Phase Transitions* **1994**, *47*, 183.
(9) Shibayama, M.; Tanaka, T. *J. Chem. Phys.* **1992**, *97*, 6842.
(10) Shibayama, M.; Tanaka, T. *J. Chem. Phys.* **1995**, *102*, 9392.
(11) Takushi, E.; Asato, L.; Nakada, T. *Nature* **1990**, *345* 298.
(12) Masuike, T.; Taki, S.; Hara, K.; Kai, S. *Jpn. J. Appl. Phys.* **1995**, *34*, 4997.
(13) Koshoubu, N.; Kanaya, H.; Hara, K.; Taki, S.; Takushi, E.; Matsushige, K. *Jpn. J. Appl. Phys.* **1993**, *32*, 4038.
(14) Hara, K.; Masuike, T.; Nakamura, A.; Okabe, H.; Hiramatsu, N. *Jpn. J. Appl. Phys.* **1995**, *34*, 5700.
(15) Hara, K.; Nakamura, A.; Hiramatsu, N.; Matsumoto, A. *Physica* **1999**, *B263−264*, 350.
(16) Sugiyama, M.; Kuwajima, S.; Soejima, Y.; Nakamura, A.; Hiramatsu, N.; Kikukawa, T.; Suzuki, A.; Hara, K. *Jpn. J. Appl. Phys.* **1999**, *38*, L1360.
(17) Sugiyama, M.; Annaka, M.; Motokawa, R.; Kuwajima, S.; Hara, K. *Physica* **2002**, *B311*, 90.
(18) Koehler, W. C. *Physica (Utrecht)* **1986**, *B137*, 320.
(19) Wignall, G. D.; Bates, F. S. *J. Appl. Crystallogr.* **1987**, *20*, 28.
(20) Sugiyama, M.; Maeda, Y. *Jpn. J. Appl. Phys.* **1994**, *33*, 6396.
(21) Koberstein, J. T.; Picot, C.; Benoît, H. *Polymer* **1985**, *26*, 673.
(22) Mallam, S.; Horkay, F.; Hecht, A. M.; Rennie, A. R.; Geissler, E. *Macromolecules* **1991**, *24*, 543.
(23) Matsuura, T.; Sugiyama, M.; Annaka, M.; Hara, Y.; Okano, T. *Polymer*, in press.
(24) Debye, P.; Bueche, A. M. *J. Appl. Phys.* **1949**, *20*, 518.
(25) Debye, P.; Anderson, H. R.; Brumberger, H. *J. Appl. Phys.* **1957**, *28*, 679.
(26) Schosseler, F.; Skouri, R.; Munch, J. P.; Candau, S. J. *J. Phys. II (Fr)* **1994**, *4*, 1221.
(27) Mendes, E.; Schosseler, F.; Isel, F.; Boué, F.; Bastide, J.; Candau, S. J. *Europhys. Lett.* **1995**, *32* (3), 273.
(28) Borue, V.; Erukhimovich, I. *Macromolecules* **1988**, *21*, 3240.
(29) Joanny, J. F.; Leibler, L. *J. Phys. (Fr.)* **1991**, *51* 545.
(30) Schosseler, F.; Moussaid, A.; Munch, J. P.; Candau, S. J. *J. Phys. II (Fr.)* **1991**, *1*, 1197.
(31) Annaka, M.; Shibayama, M.; Ikkai, F.; Sugiyama, M.; Hara, K.; Nakahira, T.; Tanaka, T. *J. Chem. Phys.* **2001**, *114*, 6906.